Stretchable Magnetoelectronics

ARTICLE *in* NANO LETTERS · JUNE 2011

Impact Factor: 13.59 · DOI: 10.1021/nl201108b · Source: PubMed

8 AUTHORS, INCLUDING:

Alfredo Calvimontes
BSH Hausgeräte GmbH
78 PUBLICATIONS **243** CITATIONS
SEE PROFILE

Daniil Karnaushenko
Leibniz Institute for Solid State and Material…
30 PUBLICATIONS **191** CITATIONS
SEE PROFILE

Stefan Baunack
Leibniz Institute for Solid State and Material…
114 PUBLICATIONS **1,143** CITATIONS
SEE PROFILE

Rainer Kaltofen
Leibniz Institute for Solid State and Material…
59 PUBLICATIONS **802** CITATIONS
SEE PROFILE

NANO LETTERS

LETTER

pubs.acs.org/NanoLett

Stretchable Magnetoelectronics

Michael Melzer,[†,∥] Denys Makarov,[*,†] Alfredo Calvimontes,[‡] Daniil Karnaushenko,[†] Stefan Baunack,[†] Rainer Kaltofen,[†] Yongfeng Mei,[§] and Oliver G. Schmidt[*,†,∥]

[†]Institute for Integrative Nanosciences, IFW Dresden, Helmholtzstrasse 20, 01069 Dresden, Germany

[‡]Leibniz Institute of Polymer Research Dresden, Hohe Str. 6, 01069 Dresden, Germany

[§]Department of Materials Science, Fudan University, 220 Handan Road, Shanghai, 200433, Peoples's Republic of China

[∥]Material Systems for Nanoelectronics, Chemnitz University of Technology, Reichenhainer Strasse 70, 09107 Chemnitz, Germany

Supporting Information

ABSTRACT: We fabricated [Co/Cu] multilayers revealing a giant magnetoresistance (GMR) effect on free-standing elastic poly(dimethylsiloxane) (PDMS) membranes. The GMR performance of [Co/Cu] multilayers on rigid silicon and on free-standing PDMS is similar and does not change with tensile deformations up to 4.5%. Mechanical deformations imposed on the sensor are totally reversible, due to the elasticity of the PDMS membranes. This remarkable performance upon stretching relies on a wrinkling of GMR layers on top of the PDMS membrane.

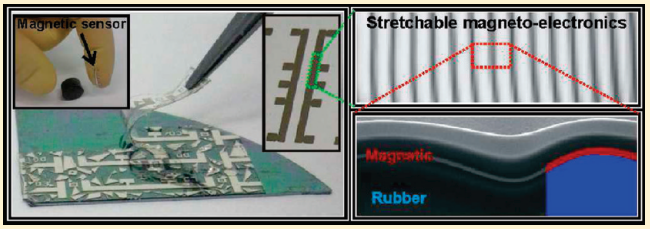

KEYWORDS: Magnetoelectronics, elastic GMR sensor, stretchable electronics, flexible electronics

Flexible electronic systems have gained substantial interest over the last years due to exciting new applications offered by arbitrary surface geometries possible after fabrication. Examples are flexible architectures of paper-like electronic displays,[1] light-emitting diodes,[2] full color display panels,[3,4] integrated circuitry,[5] solar cells,[6,7] and actuators.[8] Even stretchable electronics[9,10] and optoelectronics[11] that facilitate elastic tensile deformations have been developed for a few years. The aim of the present work is to add a new member to the family of stretchable electronics (Figure 1)—the flexible and stretchable magnetic sensor. Magnetic sensor devices on elastic substrates could enable fabrication of smart biomedical systems,[12] where large-angle folding of the micrometer-sized functional elements is a crucial prerequisite for a successful implementation.[13,14] Furthermore, flexible magnetic sensors can be directly integrated into already existing stretchable electronic systems to realize smart hybrid magnetoelectronic devices with the functionality to sense and to respond to a magnetic field.

Layered magnetic structures revealing a giant magnetoresistance (GMR) effect are crucial components of magnetic sensor devices for example in read heads for magnetic data storage[15] or in nonvolatile memory devices.[16] Currently, GMR sensors are fabricated on rigid inorganic substrates. Although there is some activity toward stretching of spin valve structures grown on rigid substrates by means of bending, the maximal achievable strain in the order of 0.1%[17,18] is too low for any applications in stretchable and flexible electronics, where strain in the percentage range is stringently required. The fabrication of GMR films on a variety of plastic substrates was reported, previously,[19,20] with GMR characteristics similar to those measured for films deposited on silicon. The effect of bending on the GMR performance was investigated only recently.[21] The influence of tensile deformations on the GMR effect of [Co/Cu] multilayers grown on conventional transparency was studied by Chen et al.[21] However, as these investigations were performed on nonelastic polymer substrates, the application of tensile strain was irreversible. More recently, Barraud et al.[22] demonstrated tunneling magnetoresistive (TMR) sensors on a polymeric substrate, but stretching of the devices was not reported.

Here, we study the performance of [Co/Cu] GMR multilayers prepared on free-standing elastic Poly(dimethylsiloxane) (PDMS) rubber membranes. We show that the GMR performance of [Co/Cu] multilayers on rigid silicon substrates and on free-standing PDMS is comparable and does not change with tensile deformations up to 4.5%. All mechanical deformations imposed on these sensor elements are reversible due to the elasticity of the used substrates. The remarkable performance of the GMR multilayers upon stretching relies on a pronounced wrinkling effect when releasing the GMR layer/rubber membrane from the substrate. The functionality of the stretchable GMR sensor was demonstrated on a proof-of-concept level by attaching it to a curved surface and measuring the sensor's response to a magnetic field of a rotating permanent magnet (Supplementary video 1, Supporting Information).

In order to fabricate GMR layer stacks on a free-standing rubber membrane, PDMS (Sylgard 184) was first spin-coated

Received: April 1, 2011
Revised: April 28, 2011
Published: May 10, 2011

dx.doi.org/10.1021/nl201108b | *Nano Lett.* 2011, 11, 2522–2526

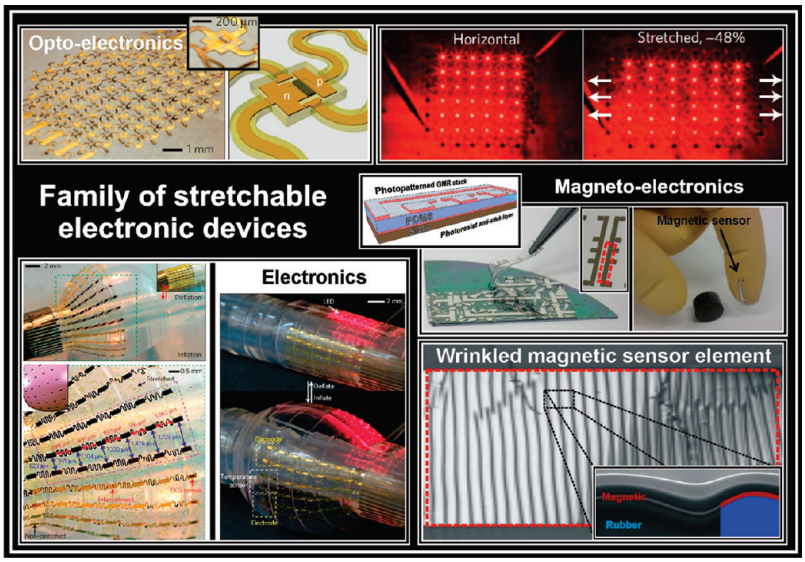

Figure 1. Family of stretchable electronic devices: (top panel) stretchable optoelectronics,[10] array of light emitting diodes (LEDs); (bottom left) stretchable electronics,[11] multifunctional inflatable balloon catheters; (bottom right) new member of the family—stretchable magnetoelectronics, giant magnetoresistive (GMR) sensor element on a free-standing PDMS membrane. Stretchability of the magnetic sensor element is due to wrinkle formation.

onto silicon wafers. Optionally, an antistick photoresist layer was introduced to assist peeling the PDMS film from the rigid silicon support. The PDMS precursor blend was cured in an oven at 90 °C for 30 min under continuous nitrogen flow, resulting in a rubber film thickness of 40 μm. GMR multilayer stacks consisting of Co(1 nm)/[Co(1 nm)/Cu(1.2 nm)]$_{50}$ were grown on the elastic PDMS surface using magnetron sputter deposition at room temperature (base pressure, 7.0×10^{-7} mbar; Ar sputter pressure, 7.5×10^{-4} mbar; deposition rate, 2 Å/s). The PDMS film was then peeled from the rigid silicon wafer leading to a free-standing elastic membrane covered with GMR multilayers. In addition, photolithographic patterning on the PDMS surface before deposition of the metal films was performed to allow for electrical resistance measurements of the GMR films on the rubber substrates. This renders the fabrication process compatible to current microelectronic structuring procedures. Further details are given in the Supporting Information (part A).

The GMR ratio is defined as the magnetic field dependent change of the sample's resistance, $R(H_{ext})$, normalized to the value of resistance when the sample is magnetically saturated, R_{sat}: GMR$(H_{ext}) = [R(H_{ext}) - R_{sat}]/R_{sat}$. Figure 2a shows the GMR ratio measured at room temperature for [Co/Cu]$_{50}$ multilayers grown on different substrates. The GMR curves obtained from the samples prepared in the same deposition run on a rigid silicon wafer without (open square symbols) and with PDMS coating (open circle symbols) are very similar. A maximum GMR value of more than 50% is obtained on both substrates. Furthermore, the GMR signal does not change after the PDMS is peeled off the silicon wafer (Figure 2a, compare curves with open and close circle symbols).

Although the GMR performance of the devices on free-standing PDMS membranes and on PDMS-coated silicon wafers is similar, the morphology of the samples is found to be substantially different. Figure 2 shows optical micrographs of a GMR multilayer on top of the PDMS surface before (Figure 2b) and after (Figure 2c) the rubber is released from the rigid substrate. When the rubber film is still attached to the silicon wafer, the metal film is smooth (root mean square roughness

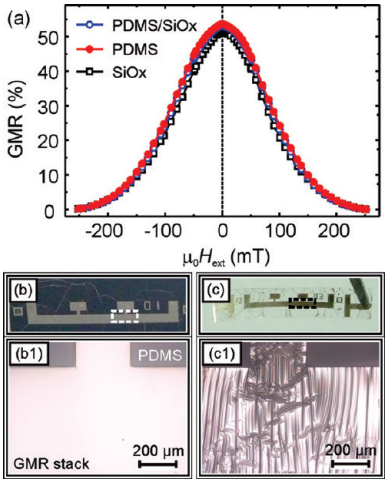

Figure 2. GMR performance of the samples: (a) GMR curves of [Co/Cu]$_{50}$ multilayers grown on different substrates: rigid SiOx wafer (open squares, resistance at zero magnetic field, R_0 = 15.3 Ω), PDMS coated silicon wafer (open circles, R_0 = 15.9 Ω) and free-standing PDMS membrane (filled circles, R_0 = 15.0 Ω). Even after the sample is peeled from the SiOx wafer, the GMR performance remains unchanged. Optical microscopy images taken from the photolithographically patterned GMR multilayers on (b) PDMS/SiOx and (c) free-standing PDMS membrane. The close-ups of the areas indicated with dashed lines in panels (b and c) are shown in panels (b1 and c1), respectively. The micrographs reveal formation of wrinkled GMR multilayer stack after the rubber was peeled from the from the SiOx wafer.

measured using atomic force microscopy (AFM) is below 1 nm (Supporting Information, part B), which indicates low intrinsic stresses during the deposition of the metal multilayers. On the free-standing rubber membrane, however, the formation of wrinkles is observed (Figure 2c). This buckling of the metal film occurs due to a contraction of the underlying PDMS upon peeling. The thermal shrinkage of the rubber film upon cooling down after curing is suppressed by the rigid silicon wafer. This

dx.doi.org/10.1021/nl201108b |*Nano Lett.* 2011, 11, 2522–2526

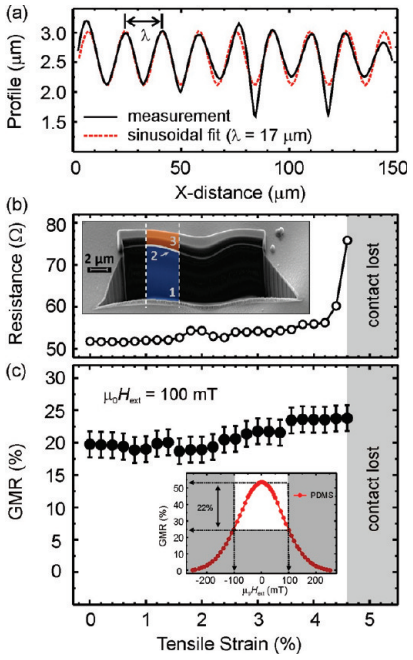

Figure 3. Wrinkled GMR multilayer stack: (a) Line scan taken of the confocal microscopy image (Supplementary Figure S3 in the Supporting Information) and the sinusoidal fit (dashed red curve) providing the wrinkle wavelength of about 17 μm. (b) Electrical resistance of the wrinkled GMR multilayer upon tensile strain. Only gradual increase in the sample resistance is observed up to 4.5% strain. Electrical contact is lost when stretching beyond 4.5%. The inset in (b) shows SEM image of a FIB cut through the sample (1, PDMS; 2, $[Co/Cu]_{50}$ multilayer stack; 3, carbon protective layer), revealing that the magnetic multilayer is firmly attached to the PDMS membrane. (c) GMR ratio in dependence of tensile strain. GMR was taken in an external magnetic field of 100 mT. Therefore, the GMR ratio of about 20% is measured in agreement with the data presented in Figure 2c (see also inset in panel c). Slight increase of the GMR ratio with tensile strain is due to the inaccuracy in applied magnetic field.

suppression is due to a large mismatch of the thermal expansion coefficients of the two materials (9.6×10^{-4} K^{-1} (PDMS) vs 2.6×10^{-6} K^{-1} (silicon)). As a result, the thermal contraction of the rubber is "stored" by means of a compressive lateral stress arising inside the PDMS. This stress is maintained during the sputter deposition of the GMR layers and is not released until the sample is peeled from the rigid supporting wafer. Upon peeling, the rubber contracts which causes wrinkling of the incompressible metal film. The formation of wrinkles after film deposition onto prestrained elastic substrates has been exploited previously for compliant electrodes, where stretchability is provided by smoothing out the buckles for lateral strains perpendicular to them.[23] The thermal contraction of the PDMS for the temperature difference of ΔT = 70 °C (from 90 °C down to room temperature), is about 7%.

The height profile of the sample reveals a wrinkling period of about 17 μm and a mean amplitude of about 0.5 μm (Figure 3a). A focused ion beam (FIB) cut of the sample (scanning electron microscopy (SEM) inset in Figure 3b) discloses the wavy GMR film (indicated by gray line) firmly attached to the bulky rubber (highlighted in blue). This suggests that the contact between the PDMS and the metal film is maintained throughout the wrinkle structure. As a result, we can apply a theoretical model by Bowden et al.[24] to estimate the period of the wrinkles, λ, formed for a thin incompressible metal film of thickness t on an elastomeric surface

$$\lambda = 4.36t\left(\frac{E_f(1-\nu_p^2)}{E_p(1-\nu_f^2)}\right)^{1/3} \quad (1)$$

here $E_{p,f}$ and $\nu_{p,f}$ denote Young's module and Poisson's ratio of the metal film (f) and the polymer (p), respectively. The values of these parameters used for the simulations are as follows: E_p = 1.6 MPa, E_f = 171 GPa ($E_{Co} \approx$ 211 GPa, $E_{Cu} \approx$ 131 GPa), ν_p = 0.48, ν_f = 0.33 (ν_{Co} = 0.31, ν_{Cu} = 0.35). The Young's modulus for the PDMS was determined from analyzing stress−strain measurements (see Supporting Information, part F), while Poisson's ratio and the data for the metal film are taken from the literature.[24−26] Considering the total thickness of the GMR multilayer stack ($t \approx$ 110 nm), the calculation according to eq 1 predicts a value for the wrinkling wavelength of $\lambda \approx$ 22 μm, which is in good agreement with the value derived from the line scan in Figure 3a. Further details are given in the Supporting Information, part C.

The free-standing PDMS rubber membranes with the photolithographically patterned and wrinkled GMR multilayers on top were mounted onto a stretching device (Supporting Information, part D). The electrical resistance of the sample upon stretching was measured using a two-probe method. It was checked that the applied stress is completely transferred to the wrinkled GMR multilayer stack (Supporting Information, part D). Figure 3b shows the measured electrical resistance while the sample was stretched. For strains of up to about 4%, only a slight increase of the samples resistance is observed. For higher strains the resistance abruptly increases and finally the electrical contact is lost at a strain of about 4.5% (gray-shaded area in Figure 3b). The increase of the resistance at higher strains is attributed to the formation of microcracks which lower the cross section of the conducting metal film. Flat metal films on top of a rubber substrate without surface wrinkling are expected to withstand tensile strains of only below 1%.[23,27]

In order to investigate the modification of the GMR effect upon stretching, at each strain value, the sample was exposed to the magnetic field of a permanent magnet. The field was chosen to be 100 mT. From the analysis of the magnetic field dependence of the $[Co/Cu]_{50}$ multilayer (Figure 2a), a GMR value of 22% is expected at $\mu_0 H_{ext}$ = 100 mT. The measured dependence of the GMR effect on the tensile strain is shown in Figure 3c. With increasing strain, only a slight change of the GMR ratio is observed, and the measured GMR ratio remains close to 20% (in agreement with the data taken on the unstrained sample, see inset in Figure 3c) even for strains of up to 4%. Tensile strains on magnetic multilayers are expected to influence the GMR effect by reducing the spacer thickness and thus varying the interlayer exchange coupling.[21,28] In our experiment however, the change of the GMR ratio upon stretching is found to be small, which indicates that tensile strain on the actual GMR multilayers is low due to the presence of the wrinkles.

The GMR sensor element is remarkably stable against cyclic loading. Figure 4a shows the resistance of a GMR multilayer on a rubber membrane during 10 stretching cycles from 0 to 1% and back. Again, a permanent magnet was employed to measure the GMR performance. For this series of measurements the magnetic field was chosen to be 300 mT to ensure that the sample was magnetically saturated. When the magnetic field is applied, the

dx.doi.org/10.1021/nl201108b |Nano Lett. 2011, 11, 2522–2526

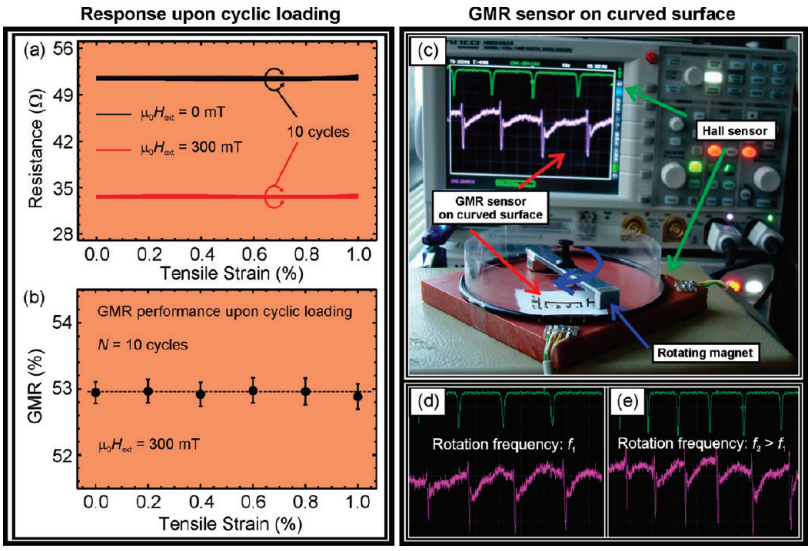

Figure 4. Performance of the elastic GMR sensor. (left panel) Response of the GMR sensor to cyclic loading: (a) resistance of the wrinkled GMR film. For the experiment, the sample was reversibly stretched (10 cycles) up to 1% of tensile strain. Resistance was measured without applied external magnetic field (black curve) and with a field of 300 mT (red curve). (b) GMR ratio in dependence of the tensile strain. Even after 10 stretching cycles up to 1% tensile strain, the GMR value remains close to the one measured for as-prepared $[Co/Cu]_{50}$ stacks grown onto PDMS/SiOx. (right panel) GMR sensor on curved surface: (c) Measurement of the magnetic field of a rotating magnet using an elastic GMR sensor attached to the curved surface of a plastic foil. When the magnet approaches the GMR sensor, a decrease of the sample resistance is observed by spikes in an oscilloscope signal (purple curve). The green curve represents the reference signal taken by a conventional Hall-effect sensor. The signal from the GMR and Hall-effect sensor are phase-shifted due to the different spatial position of both sensor elements. (d, e) Response of the GMR sensor to the rotating magnetic field of different frequencies: The increase of the rotation frequency of the permanent magnet can be easily traced with the GMR sensor.

resistance of the sample drops (Figure 4a, red curve) as expected for [Co/Cu] multilayers.[29] The resistance of the sample (with and without applied magnetic field) remains unchanged even after the sample was reversibly stretched and relaxed for 10 times (Figure 4a). Figure 4b shows the GMR ratio in dependence of the tensile strain for the cyclic loading measurements. The GMR ratio remains at a constant value of ≈53% with low deviations (±0.2%) for tensile strains up to 1% and therefore is well-suited for magnetic sensor applications in environments where deviations from a flat geometry are required.

To demonstrate the performance of the elastic GMR sensor element on a proof-of-concept level, the sensor was attached to a plastic foil shaped into a ring geometry to track the magnetic field of a rotating permanent magnet (Figure 4c). The change of the resistance of the GMR multilayer was recorded versus time (Supplementary video in the Supporting Information): When the magnet is in the proximity of the GMR sensor, a clear decrease of the sample resistance is detected (Figure 4, right panel). The dynamic response is illustrated by sensing the rotating magnetic field at higher frequency, which is easily traced with the GMR sensor (Figures 4d,e). Further details are given in the Supporting Information (part E).

In conclusion, we fabricated GMR $[Co/Cu]_{50}$ multilayers on a free-standing elastic rubber membrane revealing a strong GMR effect of more than 50%, which is comparable to the same layer stack grown on rigid silicon substrates. The GMR films on top of the elastic PDMS membrane undergo thermally induced wrinkling. These wrinkles allow for high stretchability with conductivities persisting up to 4.5% tensile strain. The GMR ratio of the sensor elements remains stable even after formation of strain-induced microcracks in the metal film. A proof-of-concept of the stretchable magnetic sensor device was presented. To further improve stretchability, mechanically instead of thermally induced prestrain might be employed to the elastomer substrates to enhance wrinkling amplitudes.

■ ASSOCIATED CONTENT

Supporting Information. Additional experimental information as well as a video demonstrating the performance of a stretchable GMR sensor. This material is available free of charge via the Internet at http://pubs.acs.org.

■ AUTHOR INFORMATION

Corresponding Author

*E-mail: d.makarov@ifw-dresden.de; o.schmidt@ifw-dresden.de.

■ ACKNOWLEDGMENT

The authors acknowledge valuable discussions with Dr. J. I. Mönch. The support in the development of the experimental setups from Dr. R. Träger is greatly appreciated. We thank I. Fiering for the assistance in the deposition of the magnetic layers, B. Eichler for the AFM imaging, and Dr. K. Schneider and H. Scheibner for mechanical characterization measurements. This work was financed via the BMBF project Nanett (federal research funding of Germany FKZ: 03IS2011F).

■ REFERENCES

(1) Rogers, J. A.; Bao, Z.; Baldwin, K.; Dodabalapur, A.; Crone, B.; Raju, V. R.; Kuck, V.; Katz, H.; Amundson, K.; Ewing, J.; Drzaic, P. *Proc. Natl. Acad. Sci. U.S.A.* **2001**, *98*, 4835–4840.

(2) Gustafsson, G.; Cao, Y.; Treasy, G. M.; Klavetter, F.; Colaneri, N.; Heeger, A. J. *Nature* **1992**, *357*, 477–479.

(3) Zhou, L.; Wanga, A.; Wu, S. C.; Sun, J.; Park, S.; Jackson, T. N. *Appl. Phys. Lett.* **2006**, *88*, 083502.

(4) Chung, I. J.; Kang, I. B. *Mol. Cryst. Liq. Cryst.* **2009**, *507*, 1–17.
(5) Kelley, T. W.; Baude, P. F.; Gerlach, C.; Ender, D. E.; Muyres, D.; Haase, M. A.; Vogel, D. E.; Theiss, S. D. *Chem. Mater.* **2004**, *16*, 4413–4422.
(6) Shaheen, S. E.; Brabec, C. J.; Sariciftci, N. S.; Padinger, F.; Fromherz, T.; Hummelen, J. C. *Appl. Phys. Lett.* **2001**, *78*, 841.
(7) Krebs, F. C.; Gevorgyan, S. A.; Alstrup, J. *J. Mater. Chem.* **2009**, *19*, 5442–5451.
(8) Kofod, G.; Wirges, W.; Paajanen, M.; Bauer, S. *Appl. Phys. Lett.* **2007**, *90*, 081916.
(9) Kim, D. H.; Ahn, J. H.; Choi, W. M.; Kim, H. S.; Kim, T. H.; Song, J.; Huang, Y. Y.; Liu, Z.; Lu, C.; Rogers, J. A. *Science* **2008**, *320*, 507–511.
(10) Kim, D. H.; Lu, N.; Ghaffari, R.; Kim, Y. S.; Lee, S. P.; Xu, L.; Wu, J.; Kim, R. H.; Song, J.; Liu, Z.; Viventi, J.; de Graff, B.; Elolampi, B.; Mansour, M.; Slepian, M. J.; Hwang, S.; Moss, J. D.; Won, S. M.; Huang, Y.; Litt, B.; Rogers, J. A. *Nat. Mater.* **2011**, *10*, 316–323.
(11) Kim, R. H.; Kim, D. H.; Xiao, J.; Kim, B. H.; Park, S. I.; Panilaitis, B.; Ghaffari, R.; Yao, J.; Li, M.; Liu, Z.; Malyarchuk, V.; Kim, D. G.; Le, A. P.; Nuzzo, R. G.; Kaplan, D. L.; Omenetto, F. G.; Huang, Y.; Kang, Z.; Rogers, J. A. *Nat. Mater.* **2010**, *9*, 929–937.
(12) Pannetier, M.; Fermon, C.; Goff, G. L.; Simola, J.; Kerr, E. *Science* **2004**, *304*, 1648.
(13) Gracias, D. H.; Tien, J.; Breen, T. L.; Hsu, C.; Whitesides, G. M. *Science* **2000**, *289*, 1170–1172.
(14) Leong, T. G.; Randall, C. L.; Benson, B. R.; Bassik, N.; Stern, G. M.; Gracias, D. H. *Proc. Natl. Acad. Sci. U.S.A.* **2009**, *106*, 703–708.
(15) Nagasaka, K. *J. Magn. Magn. Mater.* **2009**, *321*, 508–511.
(16) Prinz, G. A. *Science* **1998**, *282*, 1660–1663.
(17) Baril, L.; Gurney, B.; Wilhoit, D.; Speriosu, V. *J. Appl. Phys.* **1999**, *85*, 5139–5141.
(18) Duenas, T.; Sehrbrock, A.; Löhndorf, M.; Ludwig, A.; Wecker, J.; Grünberg, P.; Quandt, E. *J. Magn. Magn. Mater.* **2002**, *242*, 1132.
(19) Parkin, S. S. P.; Roche, K. P.; Suzuki, T. *Jpn. J. Appl. Phys.* **1992**, *31*, L1246–L1249.
(20) Parkin, S. S. P. *Appl. Phys. Lett.* **1996**, *69*, 3092.
(21) Chen, Y. F.; Mei, Y. F.; Kaltofen, R.; Mönch, J. I.; Schumann, J.; Freudenberger, J.; Klauss, H. J.; Schmidt, O. G. *Adv. Mater.* **2008**, *20*, 3224–3228.
(22) Barraud, C.; Deranlot, C.; Seneor, P.; Mattana, R.; Dlubak, B.; Fusil, S.; Bouzehouane, K.; Deneuve, D.; Petroff, F.; Fert, A. *Appl. Phys. Lett.* **2010**, *96*, 072502.
(23) Lacour, S. P.; Wagner, S.; Huang, Z.; Suo, Z. *Appl. Phys. Lett.* **2003**, *82*, 2404.
(24) Bowden, N.; Brittain, S.; Evans, A. G.; Hutchinson, J. W.; Whitesides, G. M. *Nature* **1998**, *393*, 146–149.
(25) Sanders, P. G.; Eastman, J. A.; Weertman, J. R. *Acta Mater.* **1997**, *45*, 4019–4025.
(26) Doi, H.; Fujiwara, Y.; Miyake, K.; Oosawa, Y. *Metall. Trans.* **1970**, *1*, 1417–1425.
(27) Huang, H. H.; Spaepen, F. *Acta Mater.* **2000**, *48*, 3261–3269.
(28) Sakai, T.; Miyagawa, H.; Oomi, G.; Saito, K.; Takanashi, K.; Fujimori, H. *J. Phys. Soc. Jpn.* **1998**, *67*, 3349–3352.
(29) Parkin, S. S. P. *Annu. Rev. Mater. Sci.* **1995**, *25*, 357–388.